On the Mechanism of Phenolate Photo-oxidation in Aqueous Solution.

*Alexandra L. Tyson and Jan R. R. Verlet**

Department of Chemistry, Durham University, Durham DH1 3LE, United Kingdom

Abstract

The photo-oxidation dynamics following UV (257 nm) excitation of the phenolate anion in aqueous solution is studied using broadband (550 to 950 nm) transient absorption spectroscopy. A clear signature from electron ejection is observed on a sub-picosecond timescale, followed by cooling dynamics and the decay of the signal to a constant offset that is assigned to the hydrated electron. The dynamics are compared to the charge-transfer-to-solvent dynamics from iodide at the same excitation wavelength and are shown to be very similar to these. This is in stark contrast to a previous study on the phenolate anion excited at 266 nm, in which electron emission was observed over longer time-scales. We account for the differences using a simple Marcus picture for electron emission in which the electron tunnelling rate depends sensitively on initial excitation energy. After electron emission, a contact pair is formed which undergoes geminate recombination and dissociation to form the free hydrated electron at rates that are slightly faster than for the iodide system. Our results show that, while the underlying chemical physics of electron emission differs between iodide and phenolate, the observed dynamics can appear very similar.

* j.r.r.verlet@durham.ac.uk

Introduction

Photo-oxidation is commonly observed following excitation of solute anions in the ultraviolet (UV) spectral range. For small inorganic ions, distinctive absorption bands appear in the UV that lead to charge injection into the solvent. These so-called charge-transfer-to-solvent (CTTS) bands have been extensively studied in the literature.[1–5] Perhaps the most commonly studied photo-oxidation system is the CTTS of iodide in water. With ultrafast time-resolution, the evolution of the CTTS excited state can be probed directly[3,6] as well as the subsequent solvation of the electron and radical iodine atom.[7,8] The accepted view is that, following excitation of the lowest CTTS band, a contact pair is formed which subsequently thermalizes and then decays either by geminate recombination or dissociation to form a free hydrated electron, $e^-_{(aq)}$. At higher excitation energies, the electron can be injected into the solvent at longer range.[9] Similar overall dynamics are observed for other small aqueous inorganic anions such as $Fe(CN)_6^{4-}$, for which no contact pair is formed.[10,11] In contrast, most organic molecules lack the characteristic CTTS absorption bands, but nevertheless undergo photo-oxidation,[12–14] and a question arises about how electron loss occurs in these molecules. Here we probe the photo-oxidation of the aqueous phenolate anion, $Ph^-_{(aq)}$, as a representative component of many bioactive chromophores. Using transient absorption spectroscopy, we show that, despite the absence of a CTTS band, very similar dynamics to typical CTTS processes are observed with the formation of a contact pair and subsequent dissociation and geminate recombination.

The phenolate chromophore is a common part in bioactive chromophores. For example, in photoactive proteins such as the green fluorescent protein and the photoactive yellow protein, local excitation of the $\pi^* \leftarrow \pi$ transition on Ph^- define some of the higher-lying electronic states in the UV spectral range. These have been extensively probed in the gas-phase, where very fast autodetachment has been observed.[15,16] In solution and in proteins,

photo-oxidation of many bioactive chromophores also occurs following UV excitation suggesting that the same phenolate-localised $^1\pi\pi^*$ states lead to electron loss despite the presence of a solvent or a protein.[17–22] Here, we take a bottom-up approach and probe the photo-oxidation of the simple Ph^- in aqueous solution in an attempt to understand the photochemistry of this simple chromophore as a basis to understanding the photo-oxidation more complex bioactive molecules. Specifically, we use transient absorption in the 550-950 nm spectral range to directly probe the electron loss channel through the production of hydrated contact pair and $e^-_{(aq)}$, which has a strong electronic transition around 720 nm that corresponds to its extensively studied p ← s transition.[23,24]

Ph^- has previously been studied by transient absorption. Early studies with 27 ps time-resolution, showed that $e^-_{(aq)}$ generation was essentially instantaneous.[25] More recently, the photo-oxidation of $Ph^-_{(aq)}$ has been studied in detail by the Bradforth group following excitation at 266 nm.[26] In their experiment, they probed the dynamics in the $290 < \lambda < 700$ nm range. While this study was sensitive to the $Ph^0_{(aq)}$ radical product, the sensitivity to the hydrated electron was limited because their probe only partially overlapped with that p ← s transition of $e^-_{(aq)}$ and did not access its peak. Nevertheless, they were able to deduce remarkable insight through extensive analysis and fitting of their transient data. The key conclusion from their work was that the dynamics following excitation to the S_1 $^1\pi\pi^*$ state of Ph^- did not resemble that of a typical CTTS state. Instead, a slow growth of the absorption band due to the $[Ph^0{:}e^-]_{(aq)}$ contact pair was observed, indicating a relatively slow emission of the electron from the S_1 state. In the present study, the photo-oxidation event was initiated at 257 nm (instead of 266 nm) and the resultant dynamics appear very different to the study by Chen *et al.* and instead appear similar to CTTS dynamics, implying an extreme sensitivity to excitation energy. Our results allow us to extend the interpretation provided by Chen *et al*.[26]

and provide a consistent explanation of the observed discrepancies between the two experiments.

Experimental

A home-built transient absorption setup was used to follow the ultrafast photo-oxidation dynamics of $Ph^{-}_{(aq)}$. All laser pulses were derived from a commercial Yb:KGW laser system (Carbide, Light Conversion) providing 230 fs pulses with a 84 μJ pulse energy centred around 1028 nm with a repetition rate of 60 kHz. Around 30 μJ $pulse^{-1}$ of the output was directed for use in another experiment.[27] The remaining 54 μJ $pulse^{-1}$ was used to generate the UV pump beam and white light probe for the transient absorption experiment in an approximate 19:1 ratio controlled by a half wave plate and polarising beam splitter cube.

The white light probe was generated by focusing 2-3 μJ $pulse^{-1}$ of the 1028 nm laser output into a 5 mm thick sapphire window using an aspheric lens (f = 79 mm). A key advantage of seeding the white light with 1028 nm is that the supercontinuum generated spans from the near IR (1000 nm) down to ~500 nm, without the common spectral gap centred at 800 nm from Ti:Sapphire driven continua. Hence, the resultant supercontinuum is ideally suited to probe species such as $e^{-}_{(aq)}$ and hydrated contact pairs that strongly absorb in this range. The white-light was collimated using an achromatic doublet lens (f = 30 mm) and passed through a short-pass filter to remove any residual 1028 nm. The probe was then focused by a concave mirror (f = 10 cm) into a commercial 1” sample flow cell (Harrick, DLC-M25).

The pump beam was first chopped at 30 kHz using a RTP crystal (Leysop) that switched polarisation of every other 1028 nm pulse. A subsequent polarising beam splitter was used to reflect and dump alternate pulses from the 60 kHz train. The 1028 nm fundamental was frequency converted to the fourth harmonic in two consecutive BBO

crystals, yielding 257 nm pulses with <200 fs pulse duration. The intensity of the 257 nm pump was set so that no two-photon ionisation of pure water was observed. The pump was focused by a concave mirror (f = 15 cm) onto the sample and overlapped spatially with the probe. The delay between pump and probe pulses was controlled by a commercial motorised delay stage. All experiments were conducted under magic angle (54.7°) conditions between pump and probe polarizations.

After transmittance through the sample, the probe was directed through a variable neutral density filter and a variable slit before being dispersed through a prism onto a line scan camera (Lightwise Allegro, Imaging Solutions Group). The detector was run at a line rate of 60 kHz allowing shot-to-shot measurement of pump-probe and pump off signals that are used to calculate the transient absorption spectra.

The spectra were calibrated using a commercial filter with a characteristic transmission profile (ThorLabs FGB67). The absolute wavelength assignment was on the order of ±2 nm, while the spectral resolution is ~1 nm. To characterise the chirp, a pump-probe experiment is performed on a pure solvent with the non-resonant two-photon stimulated Raman scattering signal indicating the point of pump-probe overlap for each wavelength, which was then corrected for in post-processing.

All of the results presented used a 100 mM aqueous solution of phenolate prepared by dissolving phenol (Sigma Aldrich, used without further purification) in water that was adjusted to pH = 13 using of NaOH. For iodide experiments, a 100 mM solution of NaI (Sigma Aldrich, used without further purification) in water was used. The water in all experiments was taken from a high-purity filtration unit (Millipore Milli-Q Gradient A10, 18.2 MΩ). The solution's temperature was equilibrated to that of the room at 21 °C (294 K).

Results and Analysis

The transient absorption spectra of $Ph^{-}_{(aq)}$ excited at 257 nm are shown in Figure 1. Figure 1(a) focusses on the short timescales (<5 ps) and shows the appearance of a broad absorption peak following excitation with a spectral shape that is shifting toward shorter wavelength as time evolves. The spectrum then appears to narrow on a few-picosecond timescale and decays at longer timescales as shown in Figure 1(b). The absorption spectrum at 100 ps peaks at 715 nm and can be assigned to the characteristic absorption band of $e^{-}_{(aq)}$.[7]

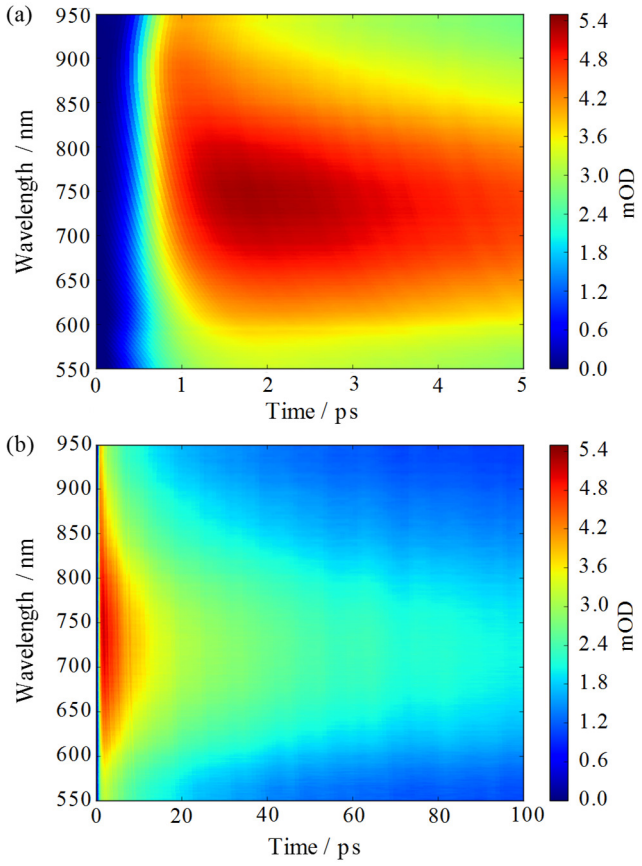

Figure 1: Transient absorption spectra of Ph^{-} excited at 257 nm, focussing on (a) dynamics at early times (5 ps) and (b) longer times (up to 100 ps).

To assist analysis of the fast dynamics, kinetic slices of the transient absorption data in Figure 1 have been taken at a series of wavelength; these are shown in Figure 2. Inspection of this data reveals two key features. The transient absorption signal across the wavelength range probed appears after ~200 fs and then peaks between approximately 1 and 2 ps, depending on the wavelength, with longer wavelengths peaking earlier (consistent with the observed blue-shift at early times in Figure 1). The overall dynamics are reminiscent of those observed for $I^-_{(aq)}$.[7,8] To explore this further, experiments on $I^-_{(aq)}$ photoexcited to its CTTS state at 257 nm were also performed.

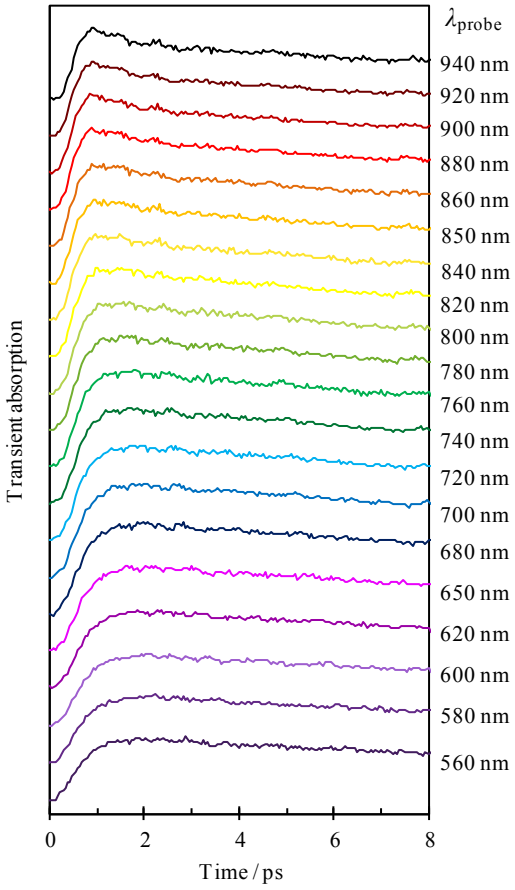

Figure 2: Kinetic traces of the transient absorption following photo-oxidation of $Ph^-_{(aq)}$ at a range of probe wavelengths.

Figure 3 shows the transient absorption kinetics of at three representative wavelengths for $I^-_{(aq)}$ and $Ph^-_{(aq)}$. Each kinetic trace has been normalised to its maximum absorption for comparison purposes. The overall kinetics following photo-oxidation of $I^-_{(aq)}$ and $Ph^-_{(aq)}$ are strikingly similar. In particular, the dynamics are very similar for short probe wavelengths and deviate somewhat as λ increases, as exemplified by the λ = 920 nm probe in Figure 3.

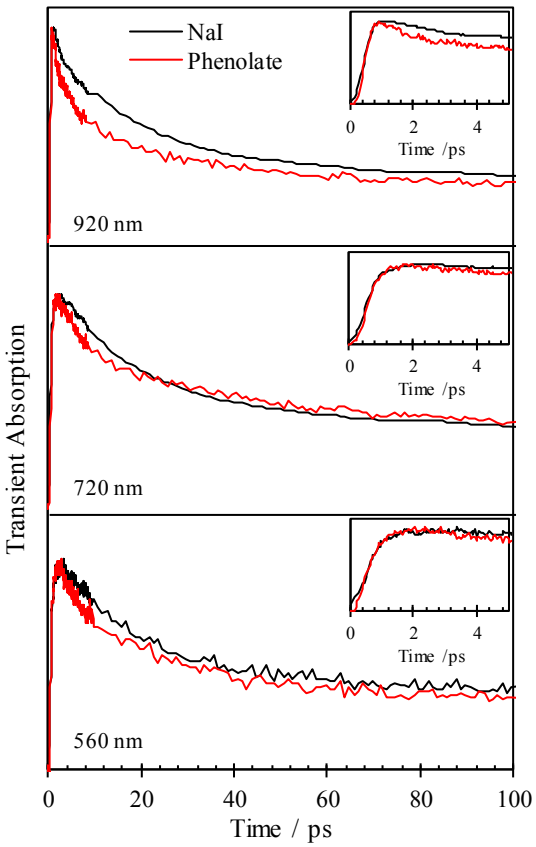

Figure 3: Normalised kinetic traces of the transient absorption at three representative probe wavelengths for following the photo-oxidation of $Ph^-_{(aq)}$ (red lines) and $I^-_{(aq)}$ (black lines). The insets show the fit to the first 5 ps of the kinetics.

Because of the overall similarity between the photo-oxidation dynamics of $I^-_{(aq)}$ and $Ph^-_{(aq)}$, we employ the model by Staib and Borgis[28,29] that has previously been used to explain the kinetics following CTTS from $I^-_{(aq)}$.[7,8] In this model, an electron is ejected from the solute with a rate constant k_p. The electron is initially located in close proximity to the radical parent

species forming a contact pair. The surrounding solvent rearranges to accommodate the altered charge distribution. Once thermalized, the contact pair can either reform the anion by nonadiabatic reverse electron transfer (geminate recombination) with rate coefficient k_n, or it can dissociate to form the neutral radical and $e^-_{(aq)}$ with a rate coefficient k_d. The contact pair and free hydrated electron are assumed to have indistinguishable absorption spectra so that the transient absorption signal can be modelled as the number density, $N(t)$, of both:

$$N(t) = \frac{k_d}{k_d + k_n} + \frac{k_p}{k_d + k_n - k_p}\left(\frac{k_p - k_d}{k_p} \exp\left(-k_p t\right) - \frac{k_n}{k_n - k_d} \exp\left(-(k_d + k_n)t\right) \right).$$

In order to fit this expression to the data in Figure 2, a convolution with the instrument response (assumed to be Gaussian with FWHM = 250 fs) was performed. While the Staib and Borgis model is useful to capture the kinetics associated with the dissociation and geminate recombination, it does not account well for the early time solvation dynamics of the hot contact pair, where spectral shifting occurs. Nevertheless, we employ the model here to demonstrate the similarity with the CTTS from both $I^-_{(aq)}$, for which the model has been previously employed.[7,8]

Fits the photo-oxidation dynamics of both $I^-_{(aq)}$ and $Ph^-_{(aq)}$ at the three representative probe wavelengths yield the resulting parameters given in Table 1. Our results for $I^-_{(aq)}$ are in good agreement with to those obtained by Bradforth and coworkers who obtained rate coefficients of $k_n = (33\ \text{ps})^{-1}$ and $k_d = (70\ \text{ps})^{-1}$ with a pump wavelength of 255 nm.[7] Overall, the kinetics for $Ph^-_{(aq)}$ fit similarly well to Eq. (1) as for $I^-_{(aq)}$, suggesting that the dynamics are also broadly similar. The formation time of the electron for $Ph^-_{(aq)}$ is comparable to $I^-_{(aq)}$, although we stress the deficiency in describing these dynamics within the model. The geminate

recombination and dissociation of the contact pair is ~25% faster on average for $Ph^-_{(aq)}$ photo-oxidation compared to $I^-_{(aq)}$.

Table 1: Lifetimes of electron production (k_p^{-1}), nonadiabatic geminate recombination (k_n^{-1}), and contact pair dissociation (k_d^{-1}) following photo-oxidation of $Ph^-_{(aq)}$ and $I^-_{(aq)}$ at 257 nm, determined from fitting the data to Eq. (1).

	Phenolate			Iodide		
λ_{probe} / nm	k_p^{-1}/ ps	k_n^{-1}/ ps	k_d^{-1}/ ps	k_p^{-1}/ ps	k_n^{-1}/ ps	k_d^{-1}/ ps
560	0.58	26	50	0.65	35	65
720	0.57	28	41	0.53	36	71
920	0.27	28	28	0.12	25	60

Discussion

The kinetics following CTTS from for $I^-_{(aq)}$ have previously been considered in detail by the Bradforth group following excitation at 255 nm[7] and were adequately captured by the model proposed by Staib and Borgis up to ~100 ps.[28,29] At longer-times, a slow additional decay of the electron signal arises from the diffusional dynamics of the dissociated $I^0_{(aq)}$ and $e^-_{(aq)}$ leading to secondary geminate recombination. The same is observed here for both $I^-_{(aq)}$ and $Ph^-_{(aq)}$, but is not considered further because our main interest is in uncovering the photo-oxidation mechanism, and these slow dynamics has been discussed in detail in the literature for other systems.[30]

While the transient absorption spectra measured here for $I^-_{(aq)}$ excited at 257 nm are very similar to those observed by the Bradforth group, the photo-oxidation of $Ph^-_{(aq)}$ by Chen *et al.* has strikingly different dynamics than those observed here. Specifically, they observed a biphasic growth in electron absorption signal that reached a maximum at ~10 ps. Their interpretation was that the initially excited S_1 state undergoes a competition between rapid electron ejection and internal vibrational relaxation in the S_1 state, as some excess vibrational

energy was imparted upon excitation (S_1 origin is at $\lambda \sim 290$ nm). The ejection from the equilibrated S_1 state would then lead to additional electron emission over a longer timescale. The electron was assumed to be ejected as a close contact pair, $[Ph^0:e^-]_{(aq)}$. This latter part is consistent with our observations, while the other aspects of the data are not. Perhaps the main punch-line of the study by Chen *et al*. was the dramatically different photo-oxidation dynamics observed for $Ph^-_{(aq)}$ compared to more commonly studied aqueous inorganic ions such as I^-,[7,8] OH^-,[31] $Fe(CN)_6^{4-}$,[10] NCS^-,[32] and to multiphoton ionisation of water.[9,33] So why are the dynamics observed here for $Ph^-_{(aq)}$ apparently contradictory to this conclusion?

To eliminate the possibility that any differences may be an artefact of the faster repetition rate of our experiment (resulting in possible incomplete relaxation between laser shots), we conducted an experiment at 1 kHz, which showed identical behaviour. Additionally, other control experiments in which we varied pump power and sample concentration had no impact. Therefore, the key difference appears to simply be the slightly different excitation wavelengths used, suggesting that the photo-oxidation mechanism of has a non-trivial dependence on the excitation energy.

Despite the apparent discrepancy between our results and those of Chen *et al*., we attempted to analyse our data using their methodology. Specifically, we focussed on the 650 nm kinetics for which the two probe ranges overlap. We could not replicate the early dynamics in our data using their model. Instead, we essentially only see fast ejection similar to CTTS dynamics suggesting that rapid electron emission from the S_1 state dominates the dynamics and this outcompetes internal vibrational relaxation in S_1. Fast ejection is also seen in the photo-oxidation of the naphtholate anion, indole, tryptophan and aniline derivatives.[25,34–36] The relatively slow signal growth attributed to the formation of the contact pair following electron ejection from the thermalized S_1 state observed by Chen *el al*. is not observed here. Note that at 650 nm, there is also a small contribution to the overall signal from S_1 absorption to higher-

lying excited states, but the presence of this does not impact our conclusions.[26] The extreme sensitivity of the branching ratio of direct emission and S_1 thermalisation to a small change in vibrational energy content in S_1 (an additional ~1300 cm^{-1}) points to the mechanism that is very sensitive to excess vibrational energy, which would be consistent with the electron emission involving tunnelling.

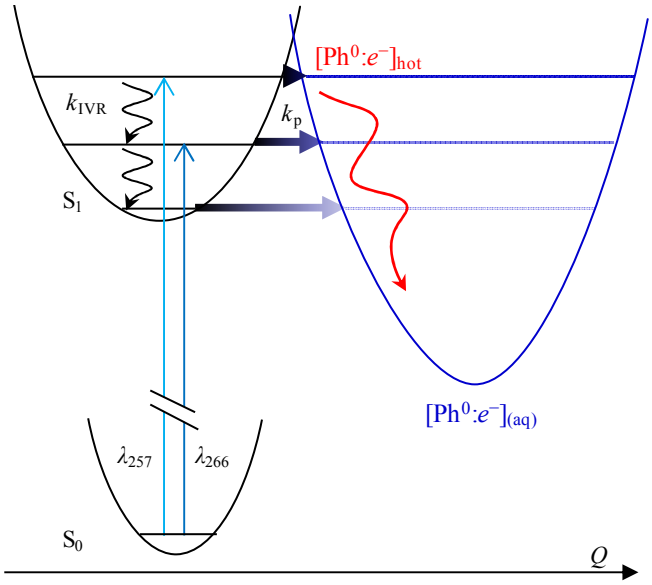

Figure 4: Schematic free energy profiles of phenolate anion along a solvent coordinate, Q. As the excitation energy increases and accesses higher vibrational levels of S_1, the tunnelling rate (k_p) of the electron to form a hot contact pair increases and outcompetes the internal vibrational relaxation rate (k_{IVR}) on S_1. Once the hot contact pair is formed, it cools to form the equilibrated contact pair.

In Figure 4, a Marcus-style schematic of free energy curves along a solvent rearrangement coordinate are sketched to aid in the following discussion, which aims to reconcile the differences in the photo-oxidation of $Ph^-_{(aq)}$ observed at 257 and 266 nm. The contact pair free energy is displaced along the solvent coordinate, Q, as solvent rearrangement is clearly necessary to achieve this. The final free energy of the contact pair is lower than that

of the S_1 state, but much higher than that of S_0 (the reverse electron transfer to reform the S_0 from the contact pair is likely to be in the inverted region). As predicted by Marcus theory, there exists a barrier between the S_1 state and the contact pair along the solvent coordinate. To form $[Ph^0:e^-]_{(aq)}$ requires electron tunnelling through this barrier. As tunnelling is very sensitive to the height and width of the barrier ($P_{\text{tunnel}} = \exp(-2\beta Q)$, where $\beta = \sqrt{2m_e(V-E)}/\hbar$), we observe a very sensitive dependence on excitation energy. At 257 nm, we are apparently close to the top of the barrier and tunnelling is sufficiently fast that it outcompetes the intramolecular vibrational relaxation on the S_1 state. At 266 nm, which is ~1300 cm^{-1} lower in energy, the barrier is larger (both in height and width) and the rate of tunnelling has slowed sufficiently so that vibrational relaxation can compete. As discussed by Chen *et al*.,[26] at 266 nm a fraction of the hot S_1 forms the contact pair rapidly, while the remainder cools on the S_1 state and this further lowers in energy. As the vibrational energy is dissipated, the tunnelling rate decreases rapidly because the barrier height and width increases (see Figure 4). Electrons are subsequently emitted at a longer timescale from the thermalised S_1 state. This emission from thermalised S_1 leads to the slow growth of absorption attributed to $[Ph^0:e^-]_{(aq)}$ formation. The final hydrated electron yield in both experiments is similar because the yield of contact pair formation is similar: the thermalized S_1 state in the experiments of Chen *et al*. still leads to electron emission. The current simple Marcus picture is fully consistent both with our data and that of Chen *et al*.. So, although the observed dynamics appear very different at the two different excitation wavelengths, the basic mechanism has the same origin.

The possibility that the mechanism can be viewed as direct autodetachment can be ruled out on energetic grounds. The photoelectron spectrum of $Ph^-_{(aq)}$ has been measured in a liquid microjet and showed that the lowest vertical detachment energy is 7.8 eV, with the adiabatic onset from the spectrum around 5.5 eV (or higher[37]). The photon energy used here (257 nm) is 4.82 eV, which is some way below the adiabatic detachment energy.

The rate of the observed electron appearance is the rate of tunnelling (related to k_p in Figure 4). Given the close agreement between the transient absorption data on $Ph^-_{(aq)}$ and $I^-_{(aq)}$ (Figure 3, Table 1), we conclude that the electron appearance time is similar to that seen for the CTTS state of and $I^-_{(aq)}$, which Vilchiz *et al.* determined to be 210 fs.[38] Immediately following tunnelling, the electron is formed as a close contact pair, which, according to Figure 4, is formed in a non-equilibrium solvent geometry. The early time-blue shift observed in Figure 1 represents the thermalisation of this hot contact pair, $[Ph^0:e^-]_{hot}$. These dynamics are again consistent with those observed following CTTS of aqueous iodide. Vilchiz *et al.* observed full thermalisation of the contact pair in ~6 ps. Here, we observe similar timescales that converge to a final absorption maximum of 715 nm of the free hydrated electron at 294 K.[23]

The similarity between CTTS dynamics of $I^-_{(aq)}$ and electron emission by tunnelling from S_1 of $Ph^-_{(aq)}$ is remarkable because the underlying mechanism for electron emission is different in both cases. The CTTS process involves a specific excited state formed by detachment into the solvent in preformed cavities.[39] For $Ph^-_{(aq)}$, this is not the case and the initial state is the S_1 $^1\pi\pi^*$ excited state of Ph^-. Bradforth and Jungwirth have shown that orbital associated with the CTTS state is predominantly of s-character.[39] In the case of Ph^- tunnelling, the S_1 state involves π orbitals and, from an isolated gas-phase perspective, we may anticipate that this will lead to emission of electrons with predominantly p-character.[40–42] The main differences between $Ph^-_{(aq)}$ and $I^-_{(aq)}$ occur at the longest wavelengths (see Figure 3). This spectral region is the most sensitive to the initially formed non-equilibrium contact pair, $[Ph^0:e^-]_{hot}$, and therefore electron ejection mechanism. Nevertheless, the rising edge at all wavelengths is very similar (see inset of Figure 3) between $Ph^-_{(aq)}$ and $I^-_{(aq)}$. This is surprising because Ph^0 has a large dipole-moment which one might anticipate would influence the ejection mechanism,[43–46] but apparently does not on the timescale of our experiment.

The cooling rate of $[Ph^0:e^-]_{hot}$ is comparable to $[I^0:e^-]_{hot}$ with the largest differences again at longest wavelengths, where the transient absorption is most sensitive to the cooling dynamics. Differences here may be anticipated. As already commented, the Ph^0 radical a large dipole moment so that the electron will presumably be predominantly localised on the positive end of this dipole (opposite to the oxygen) and so is highly directional which is not the case for CTTS from $I^-_{(aq)}$ (except at the water/air interface).[6] We also note that $Ph^0_{(aq)}$ may be produced with excess vibrational energy. This energy must also be dissipated, in contrast to I^0 which is formed in the ground state, and may lead to differences in the cooling dynamics.

Once the equilibrated contact pair is formed, the kinetics of $[Ph^0:e^-]_{(aq)}$ appear to follow those predicted by Staib and Borgis,[28,29] but faster than for $[I^0:e^-]_{(aq)}$, although not dramatically so. It is also noteworthy that the final yield of $e^-_{(aq)}$ is similar for $[Ph^0:e^-]_{(aq)}$ and $[I^0:e^-]_{(aq)}$. The faster geminate recombination kinetics are consistent with the Marcus picture, where we may anticipate that this process is in the inverted region. The larger electron affinity of I^0 compare to Ph^0 suggests that the nonadiabatic geminate recombination to form I^- is further in the inverted region and, hence, has a larger barrier so that k_n for $[Ph^0:e^-]_{(aq)}$ may be expected to be larger than for $[I^0:e^-]_{(aq)}$, consistent with the experimental observations. That k_d is also larger suggests that the free energy well for $[Ph^0:e^-]_{(aq)}$ is shallower than that of $[I^0:e^-]_{(aq)}$.

Finally, we comment that phenolate is a key chromophore in many bioactive chromophores that can undergo photo-oxidation. Examples include the green fluorescent protein and photoactive yellow protein chromophores. The photo-oxidation of the chromophores and proteins have previously been studied following UV excitation.[17–22] As we have shown recently, the excited states accessible in the UV range involve $\pi^* \leftarrow \pi$ transitions localised on Ph^-,[40] so that the chemical picture developed for photo-oxidation in the present experiments may be representative of a large class of bio-active molecules. We are currently probing the photo-oxidation of a range of such molecules.

Conclusion

The photo-oxidation of aqueous phenolate anions following excitation at 257 nm have been measured by transient absorption spectroscopy. In contrast to a previous study from the Bradforth group that studied the same process following excitation at 266 nm, the present data shows a sub-picosecond generation of a contact pair, akin to the dynamics observed for charge-transfer-to-solvent (CTTS) excitations of iodide. We account for this discrepancy using a Marcus model in which electron tunnelling leads to the formation of a contact pair, where the tunnelling is sensitively dependent on excitation energy. The contact pair is formed in a non-equilibrium (hot) solvent geometry and the transient absorption spectra clearly identify the subsequent cooling to form the equilibrium contact pair. At longer times, we observe the well-studied competitive dissociation/recombination kinetics, which again are similar to that seen following CTTS excitation of aqueous iodide, albeit faster. The photo-oxidation model presented here for the phenolate anion can be viewed as a bottom-up picture of the photo-oxidation of many photoactive proteins that have phenolate as a chromophore, in particular for the higher-lying excited states, which are most actively involved in photo-oxidation.

Acknowledgements

We thank Caleb Jordan for assistance in the experimental work on sodium iodide. This work was funded by the European Research Council (No. 306536). A. L. Tyson was supported by the Durham Doctoral Scholarship scheme.

References

(1) Barthel, E. R.; Schwartz, B. J. Mapping out the Conduction Band under CTTS Transitions: The Photodetachment Quantum Yield of Sodide (Na−) in Tetrahydrofuran. *Chem. Phys. Lett.* **2003**, *375* (3), 435–443.

(2) Bragg, A. E.; Schwartz, B. J. Ultrafast Charge-Transfer-to-Solvent Dynamics of Iodide in Tetrahydrofuran. 2. Photoinduced Electron Transfer to Counterions in Solution. *J. Phys. Chem. A* **2008**, *112* (16), 3530–3543.

(3) Messina, F.; Bräm, O.; Cannizzo, A.; Chergui, M. Real-Time Observation of the Charge Transfer to Solvent Dynamics. *Nat. Commun.* **2013**, *4*, 2119.

(4) Shoshana, O.; Lustres, J. L. P.; Ernsting, N. P.; Ruhman, S. Mapping CTTS Dynamics of Na− in Tetrahydrofurane with Ultrafast Multichannel Pump–Probe Spectroscopy. *Phys. Chem. Chem. Phys.* **2006**, *8* (22), 2599–2609.

(5) Takahashi, N.; Sakai, K.; Tanida, H.; Watanabe, I. Vertical Ionization Potentials and CTTS Energies for Anions in Water and Acetonitrile. *Chem. Phys. Lett.* **1995**, *246* (1), 183–186.

(6) Nowakowski, P. J.; Woods, D. A.; Verlet, J. R. R. Charge Transfer to Solvent Dynamics at the Ambient Water/Air Interface. *J. Phys. Chem. Lett.* **2016**, *7* (20), 4079–4085.

(7) Kloepfer, J. A.; Vilchiz, V. H.; Lenchenkov, V. A.; Germaine, A. C.; Bradforth, S. E. The Ejection Distribution of Solvated Electrons Generated by the One-Photon Photodetachment of Aqueous I− and Two-Photon Ionization of the Solvent. *J. Chem. Phys.* **2000**, *113* (15), 6288–6307.

(8) Chen, X.; Bradforth, S. E. The Ultrafast Dynamics of Photodetachment. *Annu. Rev. Phys. Chem.* **2008**, *59* (1), 203–231.

(9) Crowell, R. A.; Bartels, D. M. Multiphoton Ionization of Liquid Water with 3.0−5.0 EV Photons. *J. Phys. Chem.* **1996**, *100* (45), 17940–17949.

(10) Lenchenkov, V.; Kloepfer, J.; Vilchiz, V.; Bradforth, S. E. Electron Photodetachment from [Fe(CN)6]4−: Photoelectron Relaxation and Geminate Recombination. *Chem. Phys. Lett.* **2001**, *342* (3–4), 277–286.

(11) Shirom, M.; Stein, G. Excited State Chemistry of the Ferrocyanide Ion in Aqueous Solution. I. Formation of the Hydrated Electron. *J. Chem. Phys.* **1971**, *55* (7), 3372–3378.

(12) Feitelson, J. The Formation of Hydrated Electrons from the Excited State of Indole Derivatives. *Photochem. Photobiol.* **1971**, *13* (2), 87–96.

(13) Peon, J.; Hess, G. C.; Pecourt, J.-M. L.; Yuzawa, T.; Kohler, B. Ultrafast Photoionization Dynamics of Indole in Water. *J. Phys. Chem. A* **1999**, *103* (14), 2460–2466.

(14) Bent, D. V.; Hayon, E. Excited State Chemistry of Aromatic Amino Acids and Related Peptides. I. Tyrosine. *J. Am. Chem. Soc.* **1975**, *97* (10), 2599–2606.

(15) West, C. W.; Hudson, A. S.; Cobb, S. L.; Verlet, J. R. R. Communication: Autodetachment versus Internal Conversion from the S1 State of the Isolated GFP Chromophore Anion. *J. Chem. Phys.* **2013**, *139* (7), 071104.

(16) Mooney, C. R. S.; Horke, D. A.; Chatterley, A. S.; Simperler, A.; Fielding, H. H.; Verlet, J. R. R. Taking the Green Fluorescence out of the Protein: Dynamics of the Isolated GFP Chromophore Anion. *Chem. Sci.* **2013**, *4* (3), 921–927.

(17) Changenet-Barret, P.; Espagne, A.; Katsonis, N.; Charier, S.; Baudin, J.-B.; Jullien, L.; Plaza, P.; Martin, M. M. Excited-State Relaxation Dynamics of a PYP Chromophore Model in Solution: Influence of the Thioester Group. *Chem. Phys. Lett.* **2002**, *365* (3), 285–291.

(18) Larsen, D. S.; Vengris, M.; Stokkum, I. H. M. van; Horst, M. A. van der; Weerd, F. L. de; Hellingwerf, K. J.; Grondelle, R. van. Photoisomerization and Photoionization of

the Photoactive Yellow Protein Chromophore in Solution. *Biophys. J.* **2004**, *86* (4), 2538–2550.

(19) Vengris, M.; van Stokkum, I. H. M.; He, X.; Bell, A. F.; Tonge, P. J.; van Grondelle, R.; Larsen, D. S. Ultrafast Excited and Ground-State Dynamics of the Green Fluorescent Protein Chromophore in Solution. *J. Phys. Chem. A* **2004**, *108* (21), 4587–4598.

(20) Zhu, J.; Paparelli, L.; Hospes, M.; Arents, J.; Kennis, J. T. M.; van Stokkum, I. H. M.; Hellingwerf, K. J.; Groot, M. L. Photoionization and Electron Radical Recombination Dynamics in Photoactive Yellow Protein Investigated by Ultrafast Spectroscopy in the Visible and Near-Infrared Spectral Region. *J. Phys. Chem. B* **2013**, *117* (38), 11042–11048.

(21) West, C. W.; Bull, J. N.; Hudson, A. S.; Cobb, S. L.; Verlet, J. R. R. Excited State Dynamics of the Isolated Green Fluorescent Protein Chromophore Anion Following UV Excitation. *J. Phys. Chem. B* **2015**, *119* (10), 3982–3987.

(22) Changenet-Barret, P.; Espagne, A.; Plaza, P.; Hellingwerf, K. J.; Martin, M. M. Investigations of the Primary Events in a Bacterial Photoreceptor for Photomotility: Photoactive Yellow Protein (PYP). *New J. Chem.* **2005**, *29* (4), 527–534.

(23) Jou, F.-Y.; Freeman, G. R. Temperature and Isotope Effects on the Shape of the Optical Absorption Spectrum of Solvated Electrons in Water. *J. Phys. Chem.* **1979**, *83* (18), 2383–2387.

(24) Hart, E. J.; Boag, J. W. Absorption Spectrum of the Hydrated Electron in Water and in Aqueous Solutions. *J. Am. Chem. Soc.* **1962**, *84* (21), 4090–4095.

(25) Mialocq, J. C.; Amouyal, E.; Bernas, A.; Grand, D. Picosecond Laser Photolysis of Aqueous Indole and Tryptophan. *J. Phys. Chem.* **1982**, *86* (16), 3173–3177.

(26) Chen, X.; Larsen, D. S.; Bradforth, S. E.; van Stokkum, I. H. M. Broadband Spectral Probing Revealing Ultrafast Photochemical Branching after Ultraviolet Excitation of the Aqueous Phenolate Anion. *J. Phys. Chem. A* **2011**, *115* (16), 3807–3819.

(27) Tyson, A.; Woods, D.; Verlet, J. R. R. Time-Resolved Second Harmonic Generation with Single-Shot Phase Sensitivity. *J. Chem. Phys.* **2018**, *149*, 204201.

(28) Borgis, D.; Staib, A. Quantum Adiabatic Umbrella Sampling: The Excited State Free Energy Surface of an Electron-atom Pair in Solution. *J. Chem. Phys.* **1996**, *104* (12), 4776–4783.

(29) Staib, A.; Borgis, D. Reaction Pathways in the Photodetachment of an Electron from Aqueous Chloride: A Quantum Molecular Dynamics Study. *J. Chem. Phys.* **1996**, *104* (22), 9027–9039.

(30) Noyes, R. M. Kinetics of Competitive Processes When Reactive Fragments Are Produced in Pairs. *J. Am. Chem. Soc.* **1955**, *77* (8), 2042–2045.

(31) Crowell, R. A.; Lian, R.; Shkrob, I. A.; Bartels, D. M.; Chen, X.; Bradforth, S. E. Ultrafast Dynamics for Electron Photodetachment from Aqueous Hydroxide. *J. Chem. Phys.* **2004**, *120* (24), 11712–11725.

(32) Lian, R.; Oulianov, D. A.; Crowell, R. A.; Shkrob, I. A.; Chen, X.; Bradforth, S. E. Electron Photodetachment from Aqueous Anions. 3. Dynamics of Geminate Pairs Derived from Photoexcitation of Mono- vs Polyatomic Anions. *J. Phys. Chem. A* **2006**, *110* (29), 9071–9078.

(33) Elles, C. G.; Jailaubekov, A. E.; Crowell, R. A.; Bradforth, S. E. Excitation-Energy Dependence of the Mechanism for Two-Photon Ionization of Liquid H2O and D2O from 8.3 to 12.4 EV. *J. Chem. Phys.* **2006**, *125* (4), 044515.

(34) Feitelson, J.; Stein, G. Wavelength and Temperature Dependent Effects on Hydrated Electron Formation and Fluorescence of B-Naphtholate. *J. Chem. Phys.* **1972**, *57* (12), 5378–5382.

(35) Matsuzaki, A.; Kobayashi, T.; Nagakura, S. Picosecond Time-Resolved Spectroscopic Study of Solvated Electron Formation from the Photoexcited .Beta.-Naphtholate Ion. *J. Phys. Chem.* **1978**, *82* (10), 1201–1202.

(36) Saito, F.; Tobita, S.; Shizuka, H. Photoionization Mechanism of Aniline Derivatives in Aqueous Solution Studied by Laser Flash Photolysis. *J. Photoch. Photobio. A.* **1997**, *106* (1), 119–126.

(37) Ghosh, D.; Roy, A.; Seidel, R.; Winter, B.; Bradforth, S.; Krylov, A. I. First-Principle Protocol for Calculating Ionization Energies and Redox Potentials of Solvated Molecules and Ions: Theory and Application to Aqueous Phenol and Phenolate. *J. Phys. Chem. B* **2012**, *116* (24), 7269–7280.

(38) Vilchiz, V. H.; Kloepfer, J. A.; Germaine, A. C.; Lenchenkov, V. A.; Bradforth, S. E. Map for the Relaxation Dynamics of Hot Photoelectrons Injected into Liquid Water via Anion Threshold Photodetachment and above Threshold Solvent Ionization. *J. Phys. Chem. A* **2001**, *105* (10), 1711–1723.

(39) Bradforth, S. E.; Jungwirth, P. Excited States of Iodide Anions in Water: A Comparison of the Electronic Structure in Clusters and in Bulk Solution. *J. Phys. Chem. A* **2002**, *106* (7), 1286–1298.

(40) Anstöter, C. S.; Dean, C. R.; Verlet, J. R. R. Chromophores of Chromophores: A Bottom-up Hückel Picture of the Excited States of Photoactive Proteins. *Phys. Chem. Chem. Phys.* **2017**, *19* (44), 29772–29779.

(41) Elkins, M. H.; Williams, H. L.; Shreve, A. T.; Neumark, D. M. Relaxation Mechanism of the Hydrated Electron. *Science* **2013**, *342* (6165), 1496–1499.

(42) Bragg, A. E.; Verlet, J. R. R.; Kammrath, A.; Cheshnovsky, O.; Neumark, D. M. Hydrated Electron Dynamics: From Clusters to Bulk. *Science* **2004**, *306* (5696), 669–671.

(43) Liu, H.-T.; Ning, C.-G.; Huang, D.-L.; Dau, P. D.; Wang, L.-S. Observation of Mode-Specific Vibrational Autodetachment from Dipole-Bound States of Cold Anions. *Angew. Chem. Int. Edit.* **2013**, *52* (34), 8976–8979.

(44) Bull, J. N.; Verlet, J. R. R. Observation and Ultrafast Dynamics of a Nonvalence Correlation-Bound State of an Anion. *Sci. Adv.* **2017**, *3* (5), e1603106.

(45) Bull, J. N.; West, C. W.; Verlet, J. R. R. Ultrafast Dynamics of Formation and Autodetachment of a Dipole-Bound State in an Open-Shell π-Stacked Dimer Anion. *Chem. Sci.* **2016**, *7* (8), 5352–5361.

(46) Rogers, J. P.; Anstöter, C. S.; Verlet, J. R. R. Evidence of Electron Capture of an Outgoing Photoelectron Wave by a Nonvalence State in (C6F6)N–. *J. Phys. Chem. Lett.* **2018**.